PHYSICAL REVIEW B VOLUME 19, NUMBER 10 15 MAY 1979

Dynamical calculation of low-energy electron diffraction intensities from GaAs(110): Influence of boundary conditions, exchange potential, lattice vibrations, and multilayer reconstructions

R. J. Meyer, C. B. Duke, and A. Paton
Xerox Webster Research Center, Xerox Square-114, Rochester, New York 14644

A. Kahn, E. So, J. L. Yeh, and P. Mark
Department of Electrical Engineering, Princeton University, Princeton, New Jersey 08540
(Received 2 November 1978)

Dynamical calculations of the intensities of normally incident low-energy electrons diffracted from GaAs(110), performed using a matrix-inversion method, are compared both with earlier kinematical calculations and with measured intensities. The insensitivity of the calculated intensities to the choice of exchange potential and vacuum-solid boundary conditions is displayed. Surface lattice vibrations are found to be adequately described by the bulk Debye temperature. We consider second- and third-layer structural distortions as well as top-layer reconstructions. This analysis leads to the selection of the most probable surface structure for GaAs(110) as one in which the top layer undergoes both a rigid rotation of 27.4° and a 0.05-Å contraction with the As atoms moving outward and the Ga atoms inward, giving a relative vertical shear of 0.65 Å. In the second layer the Ga moves outward 0.06 Å and the second-layer As moves inward 0.06 Å. The dynamical analysis reported herein shows no evidence for third-layer distortions.

I. INTRODUCTION

In a series of earlier papers we described the use of dynamical[1,2] and kinematical[3,4] elastic low-energy-electron diffraction (ELEED) intensity analyses to determine the atomic geometry of GaAs(110). The early dynamical ELEED calculations[1,2] made use of the approximate renormalized-forward-scattering (RFS) method and permitted variation of only the top-layer geometry. Constant-momentum-transfer-averaged (CMTA) kinematical calculations,[3,4] however, suggest that distortions of the uppermost three atomic layers are necessary to obtain good correspondence between theory and experiment. Our purpose in this paper is the presentation of a new dynamical ELEED intensity analysis for GaAs(110) utilizing a new set of computer programs based on an approximate matrix-inversion multiple-scattering method,[5,6] which allows the examination of reconstructions of an arbitrary number of surface layers.

In addition, a number of issues have been raised in the literature in connection with reconstructions of metal surfaces which have been unresolved as regards semiconductor surfaces. Recent ELEED calculations for metals[7-9] indicate that the use of Kohn-Sham exchange[10] in the formulation of crystal potentials gives better agreement with experiment than the use of Slater exchange.[11] We have, therefore, explored the effects of model exchange potential. Our results indicate no significant difference in agreement with experiment for Kohn-Sham (KS) versus Slater exchange in GaAs(110), in contrast to the results found in metals. We also reconsider the issue, raised previously by Duke *et al.*,[12] of the influence of vacuum-solid boundary conditions on the intensity profiles obtained in ELEED calculations, and investigate the effects of a new boundary condition. Furthermore, the effects of surface vibrations are examined for the GaAs(110) surface. We conclude that surface lattice vibrations are not enhanced on the (110) semiconductor surface, as is the usual case for metal surfaces.[13,14] Finally, we compare the structure of GaAs(110), as determined from our dynamical ELEED analysis, to the structure as determined by several energy-minimization[15,16] and angular-resolved photoemission[17] methods. Unlike the case of the elemental semiconductor Si(100) $p(2\times1)$, where the dynamical ELEED structure determination gives a result incompatible with the results of the photoemission analysis,[18] we will see that our structure is in excellent agreement with that determined by other methods.

To place in perspective the issues raised above we proceed in two steps. First, in Sec. II we describe the influence on the calculated ELEED intensities of the nonstructural parameters, i.e., the construction of the crystal potentials, the modification of the atomic scattering factors to include the effects of temperature, the boundary conditions, and the method of computation. Then, in Sec. III we describe the results of the

structural analysis. In Sec. IV we summarize our results and compare them with those obtained by other methods.

II. MODEL CALCULATIONS

Since the computational procedure used in our analysis has already been described,[6] we confine our discussion of the model to the new features which have been introduced to this calculation. Specifically, in this section we consider (i) the electron-solid interaction, consisting of the evaluation of the crystal potential and the modification of the atomic scattering factors to include lattice vibrations, and (ii) the computational procedure and the effects of the choice of boundary conditions at the vacuum-solid interface. We discuss each in turn.

A. Electron-solid interaction

The crystal potentials were calculated with an overlapping-atomic-charge-density model[19] using the expression

$$V_c(r)=\frac{-Ze^2}{r}+\frac{e^2}{r}\int_0^r \sigma(t)dt+e^2\int_r^\infty \frac{\sigma(t)}{t}dt - 3\alpha e^2\left(\frac{3\sigma(r)}{32\pi^2 r^2}\right)^{1/3}, \quad (1)$$

in which $\sigma(\vec{r})$ is the crystal radial charge density resulting from a superposition of ionic charge densities. The last term in Eq. (1) is the Slater approximation[11] to the exchange energy if $\alpha=1$, and the Kohn-Sham approximation[10] to the exchange energy if $\alpha=\frac{2}{3}$. To evaluate the crystal potential we utilize the charge densities associated with singly ionic species, i.e., Ga^+As^-. The crystal structure (see Fig. 1) is that given by Wyckoff.[20] As previously[1-4] we use the muffin-tin radii $r_{MT}^{As}=1.25$ Å, $r_{MT}^{Ga}=1.20$ Å as determined from crystal potential crossover. The Wigner-Seitz radii are $r_{WS}^{As}=1.79$ Å, and $r_{WS}^{Ga}=1.72$ Å. Once the crystal potential in a given Wigner-Seitz cell has been obtained, it is reduced to muffin-tin form.

The scattering of electrons from each ion core of type ν is described by a set of phase shifts $\delta_l^\nu(E)$ which depend on the ion type and the incident electron energy. In this calculation we have considered phase shifts generated using Eq. (1) with (i) $V_c(r)$ and $\sigma(r)$ calculated using $\alpha=1$, (i.e., Slater exchange) and (ii) $V_c(r)$ and $\sigma(r)$ calculated using $\alpha=\frac{2}{3}$, [i.e., Kohn-Sham (KS) exchange]. The Slater phase shifts are shown in Fig. 2 for the Ga^+ and As^- ions. There is little difference between the Kohn-Sham and Slater phase shifts,

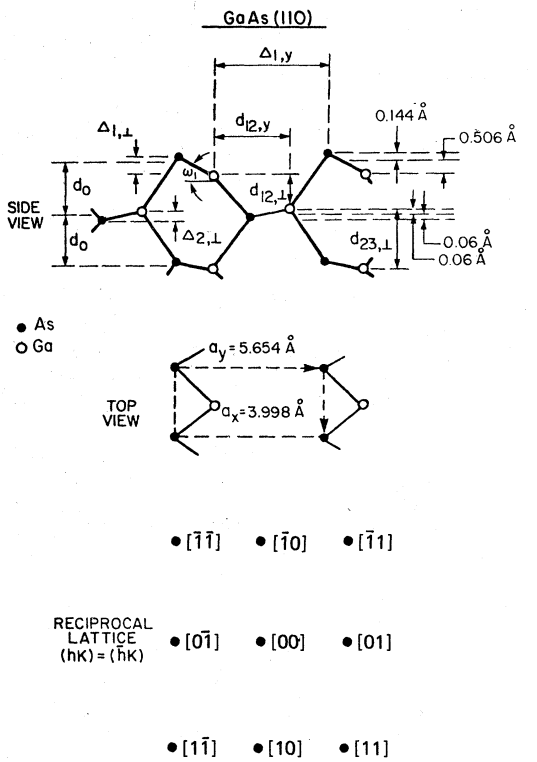

FIG. 1. Schematic indication of the surface atomic geometry and the associated ELEED normal incidence spot pattern for the (110) surface of GaAs. The symbols utilized in Table I are defined in the upper panel of the figure.

and so the Kohn-Sham phase shifts are not shown.

The optical potential associated with the electron-electron interactions is taken to be spacially uniform outside the muffin-tin spheres and of the form

$$\Sigma(E)=-V_0-i\hbar[2m(E+V_0)]^{1/2}/m\lambda_{ee}, \quad (2)$$

where V_0 is the real "inner potential" and λ_{ee} is the inelastic-collision damping length.[21] By trial and error we have chosen $V_0=10$ eV and $\lambda_{ee}=10$ Å. This procedure probably is less precise than the R-factor method,[22-24] in which the inner potential V_0 is treated on a par with the structural parameters, but is the best that can be done sensibly given the complex surface structures and modest reproducibility of ELEED data from compound semiconductors.

The final parameters which we must specify are those associated with the vibrational motion of the atomic scatterers. This motion is incorporated into the calculation of the ELEED intensities by a renormalization of the rigid-lattice electron–ion-core vertex. In the case of a rigid lattice, these vertices are given by[6]

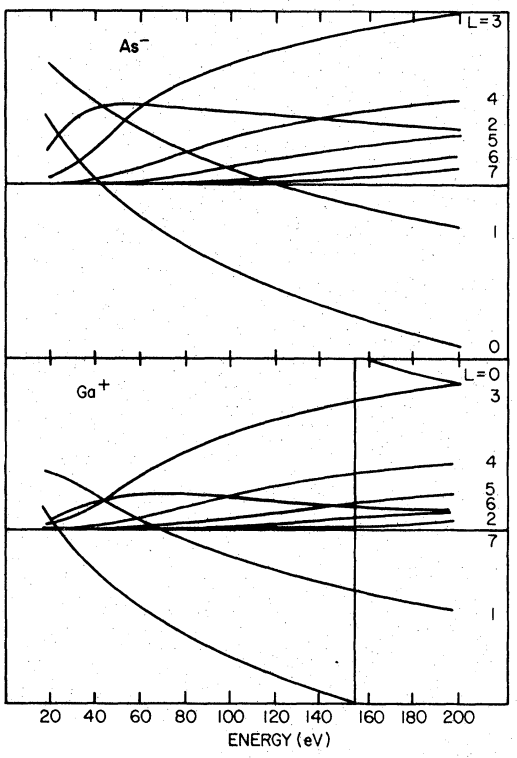

FIG. 2. Phase shifts for the Ga^+ and As^- species resulting from Slater exchange.

$$t_\nu(\vec{k}', \vec{k}) = \frac{4\pi^2 i\hbar^2}{mk(E)} \sum_{l,m} (2l+1)(e^{2i\delta_l^\nu(E)} - 1) \times Y_{lm}^*(\hat{k}') Y_{lm}(\hat{k}) , \tag{3a}$$

where

$$k_\perp^2(\vec{g}, E) = 2m[E - \Sigma(E)]/\hbar^2 - (\vec{k}_\parallel + \vec{g})^2 \tag{3b}$$

and

$$k_\parallel^2 = 2mE \sin^2\theta/\hbar^2 . \tag{3c}$$

The vector $\vec{g}$ is a vector in the surface reciprocal lattice, $\hat{k}$ is a unit vector in the direction of $\vec{k}$, and ν labels the layer parallel to the surface in which the ion core is found. The $\delta_l^\nu(E)$ may depend explicitly on this index. The consequences of atomic vibrations are introduced, in an approximate way,[25] by the multiplication of the rigid-lattice t vertices by the associated Debye-Waller factor. Using the spherical Debye model of the lattice-vibration spectra we get

$$b_\nu(\vec{k}', \vec{k}) = t_\nu(\vec{k}', \vec{k}) \exp[-(\vec{k}' - \vec{k})^2 W_\nu(T)] , \tag{4a}$$

where

$$W_\nu(T) = \frac{3\hbar^2}{2M_\nu \kappa \Theta_D^\nu} \left[\frac{1}{4} + \left(\frac{T}{\Theta_D^\nu}\right)^2 \int_0^{\Theta_D^\nu/T} \frac{x\,dx}{e^x - 1}\right] . \tag{4b}$$

In order to assess the nature of the surface-lattice vibrations on GaAs(110) we have considered three models: (i) the rigid-lattice model $T=0$, (ii) the bulk vibration model, in which $\theta_D = 345$ K for all layers, and (iii) an enhanced surface vibration model, in which $\theta_D^{\text{surface}} = 173$ K and $\theta_D^{\text{bulk}} = 345$ K. These have been compared with data taken at $T = 150$ and 300 K.

B. Boundary conditions and computational procedure

The matrix-inversion computer programs used to perform the calculations of ELEED intensities from GaAs(110) are modified versions of those described by Laramore and Duke.[6] The scattering within each subplane is calculated in the angular momentum representation by

$$\tau_\nu^{LL'}(k(E)) = b_\nu^{LL'}(k(E)) + \sum_{L_1 L_2} b_\nu^{LL_1}(k(E)) G_{L_1 L_2}^{\text{sp}}(\vec{k}_i) \times \tau_\nu^{L_2 L'}(k(E)) , \tag{5}$$

where $\sum_L = \sum_l \sum_{m=-l}^{l}$ and G^{sp} is the subplane propagator. The interference between subplanes is given by the matrix equation

$$T_\nu^{LL'}(k(E)) = \tau_\nu^{LL'}(k(E)) + \sum_{L_1 L_2} \sum_{\nu_1 \neq \nu} \tau_\nu^{LL'}(k(E)) \times G_{L_1 L_2}^{\nu\nu_1}(\vec{k}_i) T_{\nu_1}^{L_2 L'}(k(E)) , \tag{6}$$

where $G_{L_1 L_2}^{\nu\nu_1}$ is the interlayer propagator. The amplitude T_ν for all scattering processes where the final scattering event takes place in the νth layer is then given by

$$T_\nu(\vec{k}_f, \vec{k}_i) = \sum_{LL'} T_\nu^{LL'}(k(E)) Y_L^*(\hat{k}_f) Y_{L'}(\hat{k}_i) . \tag{7}$$

In this calculation we make the approximation that $T_\nu^{LL'}$, for $\nu \leq 3$, is calculated by limiting the sum over ν_1 to $\nu_1^{\max} = 3$. That is, the interlayer scattering within the top three bilayer slab, where most reconstruction occurs, is treated exactly. The interlayer scattering is ignored for the deeper layers, and we approximate $T_\nu^{LL'}$ by $\tau_\nu^{LL'}$. We limit ourselves to a six-layer calculation since the addition of further layers does not significantly change the result for the values of λ_{ee} used herein.

The approximate T-matrix calculation just described is similar to approximations used previously on GaAs. Lubinsky *et al.*[1] used a method in which the T-matrix was evaluated for the uppermost bilayer, and the RFS approximation was used for lower layers. Tong *et al.*[26] have used a similar approximation, which they call the combined-space method,[27] in which scattering within the uppermost two bilayers is solved exactly, while scattering in lower layers

is treated by the RFS method.

Turning to the topic of boundary conditions, we see that since in the inelastic collision model[21] the values of $\vec{k}$ are complex, the $Y_{lm}(\hat{k})$ in expressions like (3a) and (7) are not defined. The problem of wave propagation in an attenuating medium is a common problem in optics, e.g., the problem of refraction of a light wave at a metal surface. The accepted solution to the problem of defining trigonometric functions for complex wave vectors in optics[28] consists of utilizing functions describing the motion of surfaces of constant phase. These surfaces do not in general coincide with surfaces of constant amplitude. This choice is equivalent to choosing

$$\cos\theta_f = -\,\mathrm{Re}(k_{fz})/\mathrm{Re}(k_f) \tag{8a}$$

$$\sin\theta_f = k_{fx}/\mathrm{Re}(k_f)\,, \tag{8b}$$

or only using the real parts of k in the Y_{lm}'s. We refer to this procedure as the "optics" boundary condition. Duke *et al.*[12] have considered several possible alternate definitions of $Y_{lm}(\hat{k})$. Realizing that the exiting beam propagates in the $z<0$ direction and is continually damped, $-\bar{k}'_{\perp}(\vec{g}, E)$, a number in the lower-half complex k plane, also is physically reasonable for use in formulating $Y^*_{lm}(\hat{k}_f)$. This will be called boundary condition two, i.e., "BC2."

C. Sensitivity analysis

In any surface structure determination via ELEED intensity analysis a number of features of the model calculations are selected which are not related directly to the surface atomic geometry. In our case these include the choice of exchange potential (KS versus Slater), the inclusion of lattice vibrations (rigid-lattice versus bulk-lattice vibrations versus enhanced-surface vibrations), the choice of vacuum-solid boundary conditions (optics versus BC2), and the convergence of the approximation schemes. This subsection is devoted to an assessment of the consequences of these choices and of the uncertainties in the values of the structural parameters introduced thereby.

The first important ingredient in this assessment is the establishment of convergence of the computational scheme, both in terms of the number of phase shifts used, and the number of layers for which the T matrix is solved exactly. In Fig. 3 we show the $(1\bar{2})$ beam. From comparisons of panels (a) and (b) we see little effect for solving the T matrix for four and three layers exactly, respectively. Similarly, we see that for this beam at least, four phase shifts is a good approximation to the six-phase-shift result [panels (b) and (c)]. For comparison, we

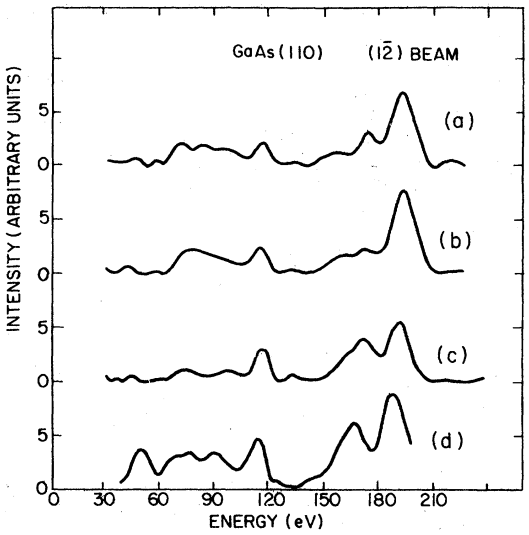

FIG. 3. Comparison of the predicted normal-incidence intensities for the $(1\bar{2})$ beam calculated using Slater exchange and a rigid lattice, with the surface structure of Tong *et al.* (Ref. 26). Curve (a): calculated intensity using four phase shifts and solving the T matrix of the top four layers exactly in Eq. (6). Curve (b): same as curve (a), only solving the T matrix of the top three layers exactly in Eq. (6). Curve (c): same as curve (b), only calculated using six phase shifts. Curve (d): intensity calculated by Tong *et al.* (Ref. 26) using the combined space method (Ref. 27). The potential and phase shifts used by Tong *et al.* were not specified in Ref. 26.

show the same beam calculated by Tong's combined-space method [panel (d)]. Our calculations suggest, therefore, that the use of four phase shifts is an adequate approximation to test the effect of variation of nonstructural parameters. We also note that the computation scheme outlined in Sec. II B converges quite well when we solve the T matrix exactly for only the top three layers.

Similarly, we must address the question of boundary conditions to be used in the diffraction calculation. Duke *et al.*[12] examined the importance of the choice of boundary conditions in ELEED calculations from metal surfaces and found that the choice was unimportant, except at low energies $E \lesssim 30$ eV. In Sec. II B we reexamined the question of vacuum-solid boundary conditions, and introduced the "optics" boundary condition. We have compared the optics boundary condition with that used in previous ELEED calculations,[5,6] labeled BC2. As in the case of metals, we found that the intensity profiles are insensitive to boundary condition choice, except at low energies, $E \lesssim 40$ eV, where the optics boundary condition enhanced peak heights by approximately 20% over those calculated with BC2. Thus throughout most of the region of

interest, the choice of boundary condition is immaterial in the analysis of surface structure. We utilize the optics boundary condition in the remainder of our calculations.

In view of the advantages claimed for KS local exchange over Slater exchange in metals,[7-9] we have examined the intensity profiles calculated using both KS and Slater models (using four phase shifts). Typical results are shown in Fig. 4 for the (01) beam, using the structure published by Tong *et al.*[26] Similar results are found on other beams, and with other trial structures. It is plain that only negligible differences exist between the intensities calculated with the different potentials. Therefore, in Sec. III we present only calculations embodying phase shifts constructed with the Slater exchange model, although we performed many calculations using KS phase shifts also.

In a recent analysis[29] of ELEED intensities from ZnO($10\bar{1}0$) we reported on the sensitivity of some beams to the presence or absence of lattice vibrations in the diffraction calculation. Due to the absence of low-temperature ELEED data for ZnO, we were unable to pursue the question of magnitude of vibrations on the semiconductor surface. Similarly, previous dynamical analyses of GaAs(110) were either carried out for a rigid lattice[1,2] or in a temperature regime where lattice vibrations were claimed to be unimportant.[26] In metals it is well known that surface vibrations are described by a Debye temperature on the order of half that of the bulk.[13,14] In GaAs it is known that some surfaces

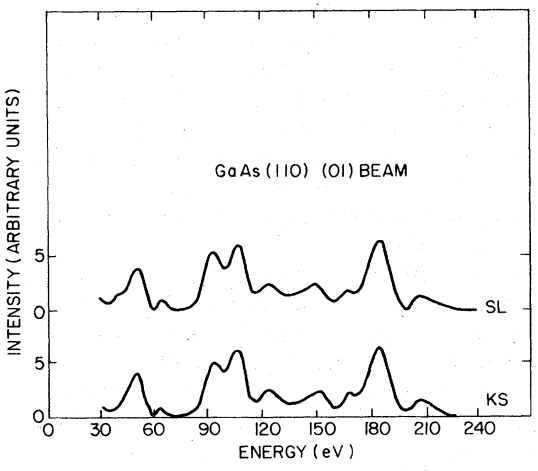

FIG. 4. Comparison of the predicted normal-incidence (01) intensities obtained using Slater exchange (SL) and Kohn-Sham exchange (KS) for the structure published by Tong *et al.* (Ref. 26). The calculations were performed using a rigid-lattice model, and four phase shifts.

are more stable than others,[30] which would correspondingly influence surface vibrations. For the these reasons we decided to explore the magnitude of lattice vibrations in GaAs(110).

ELEED data from GaAs(110) was taken for $T=150$ and 300 K for the (01), ($0\bar{1}$), (10), (11), ($1\bar{1}$), (02), ($2\bar{1}$), ($1\bar{2}$), (13), and ($1\bar{3}$) beams at normal incidence. The data acquisition has been described elsewhere,[31,32] and will not be repeated here. Temperature was found to have little effect on the experimental intensity profiles [compare panels (d) and (e), Figs. 5–14]. Lattice vibrations were incorporated into the model calculations as described above, although four phase shifts were utilized in the computations. Our final results for a variety of interesting structures and for both rigid and vibrating lattice models are presented in Figs. 5–14. Panels (d)–(f) of Figs. 5–10 reveal that the inclusion of lattice vibrations had little effect on the calculated intensity profiles of the lower order beams. For the higher-order beams, however, peaks situated at higher than 100 eV were found to virtually vanish when a model of lattice vibrations with $\Theta_D^{\text{bulk}}=345$ K, and $\Theta_D^{\text{surface}}=0.5\,\Theta_D^{\text{bulk}}$ was used, particularly for the ($2\bar{1}$) beam [see Fig. 11 panels (e) and (f)], the ($1\bar{2}$) beam [see Fig. 12, panels (e) and (f)], and the ($1\bar{3}$) beam [see Fig. 14, panels (e) and (f)]. This is in clear disagreement with experiment, as shown in panels (d) and (e). Consequently, we conclude that $\Theta_D^{\text{surface}}\approx\Theta_D^{\text{bulk}}$. To illustrate the veracity of this hypothesis, we include in panel (e) of Figs. 5–14, the intensities predicted by a model in which $\Theta_D^{\text{surface}}=\Theta_D^{\text{bulk}}=345$ K. The results are either unchanged or improved for all beams relative to those predicted by the model in which $\Theta_D^{\text{surface}}=0.5\,\Theta_D^{\text{bulk}}$.

III. STRUCTURAL ANALYSIS

Given the negligible effects of the model exchange potential and the vacuum-solid boundary conditions, we have performed our structural analysis using Slater exchange and the optics boundary condition discussed in Sec. II. Our structural analysis was performed using two vibrating lattice models described by (i) $T=300$ K with $\Theta_D=345$ K for all layers [panel (e), Figs. 5–14] and (ii) $T=300$ K with $\Theta_D=175$ K for the surface layer and $\Theta_D=345$ K for all other layers [panel (f), Figs. 5–14] for comparison with data taken at $T=300$ K. In addition, due to the effects of the model of lattice vibrations, we have calculated our final structures [panels (a)–(d), Figs. 5–14] using a rigid lattice model for comparison with data taken at $T=150$ K, where the

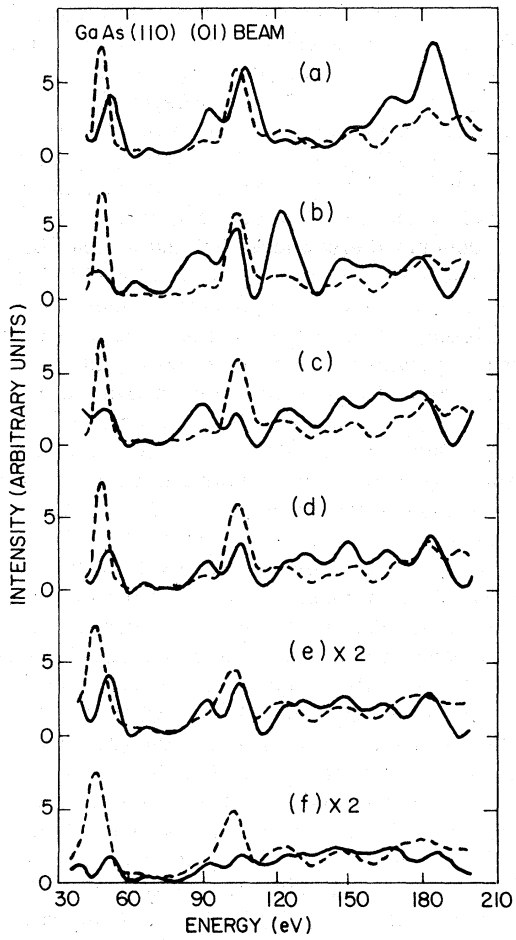

FIG. 5. Comparison of calculated (solid curves, six phase shifts) and measured (dashed curves) intensities of the (01) beam of normally incident electrons diffracted from GaAs (110). Curve (a): the measured intensity at $T = 150$ K (dashed curve) and the calculated intensity (solid curve) using the bulk geometry of Wyckoff (Ref. 20) and the first-layer distortion of Tong *et al.* (Ref. 26) for a rigid-lattice model. Curve (b): same as curve (a), but evaluated using the three-layer reconstruction of Kahn *et al.* (Ref. 4) and a rigid lattice. Curve (c): same as curve (a) but evaluated using the three-layer reconstruction of Miller and Haneman (Ref. 16) described in Table I [panel (c)] and a rigid lattice. Curve (d): same as curve (a), but evaluated using the two layer "best fit" reconstruction described in Table I [panel (d)] and a rigid lattice. Curve (e): same as curve (d), but evaluated using a lattice described by $T = 300$ K, $\Theta_D = 345$ K, and measured intensity (dashed curve) at $T = 300$ K. Curve (f): same as curve (d), but evaluated using a lattice described by $T = 300$ K, Θ_D (surface) = 173 K, Θ_D (bulk) = 345 K.

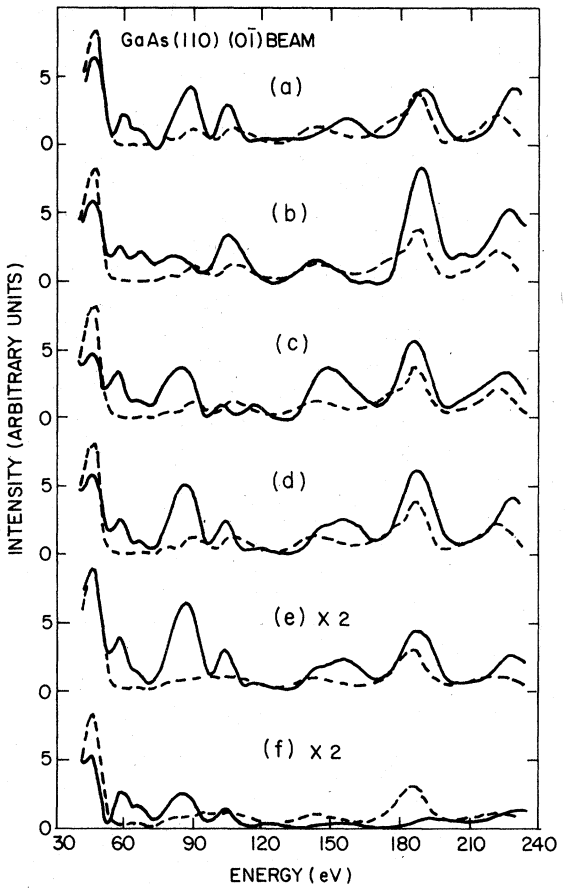

FIG. 6. Same as Fig. 5, only for the (0$\bar{1}$) beam.

effects of lattice vibrations (which are apparent at $T = 300$ K) are more modest. Initially, a complete range of single-layer reconstructions was examined corresponding to the Wyckoff[20] bulk GaAs geometry modified by rigid rotations of the top layer in the range 25°–34.8° with the As being rotated outward and the Ga inward, as shown in Fig. 1. This produced a top layer vertical shear between the As and Ga in the range 0.60–0.80 Å. Comparisons with measured ELEED intensities from 11 samples and their average [shown as the dashed curves, Figs. 5–14] were performed for the (01), (0$\bar{1}$), (10), (11), (1$\bar{1}$), (02), (2$\bar{1}$), (1$\bar{2}$), (13), and (1$\bar{3}$) diffracted beams associated with normally incident electrons.

It is worthwhile noting that the variation of individual sample intensity profiles from the average shown is generally less than ±10% for prominent peaks and better in other regions. Thus the average intensities shown adequately represent the intensity profile of any individual sample.

The initial search revealed that a top-layer rigid rotation of the As outward within the range 27°–30°, with the corresponding vertical shears of 0.65–0.70 Å, presented the most satisfactory comparisons between the calculated and observed intensities for the majority of the beams ex-

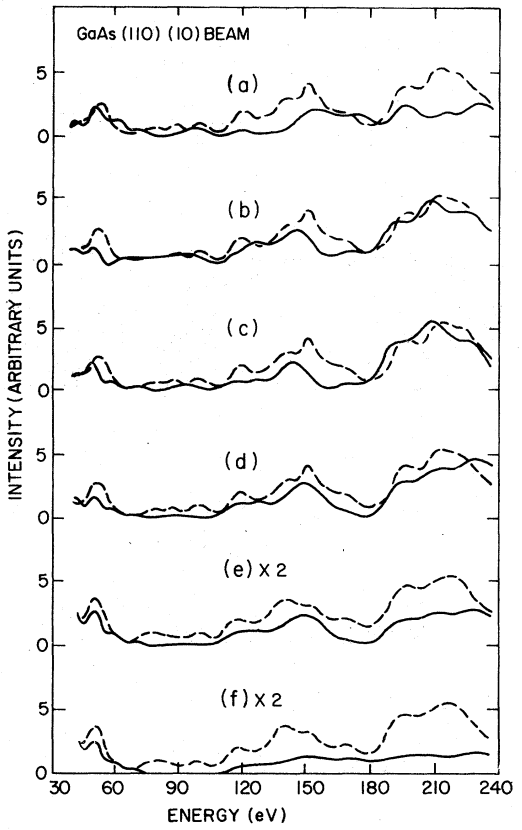

FIG. 7. Same as Fig. 5, only for the (10) beam.

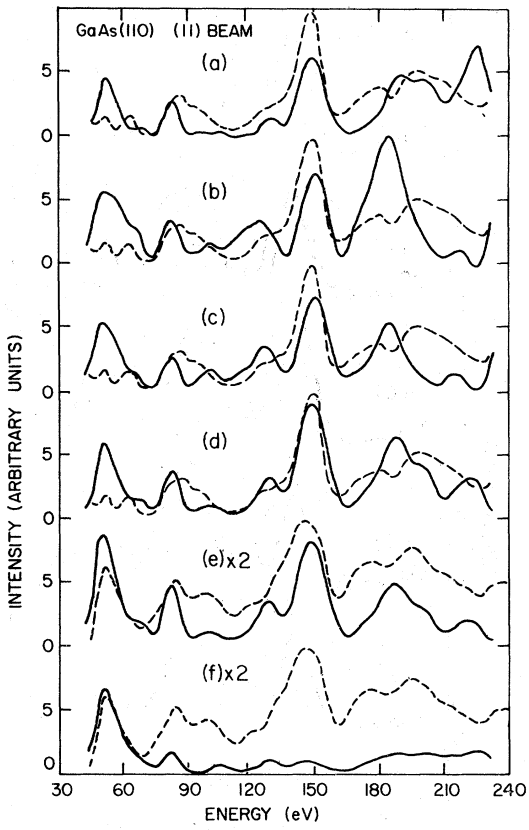

FIG. 8. Same as Fig. 5, only for the (11) beam.

amined. The (01) beam favored a larger shear of ~0.80 Å. Such a large shear tended, however, to diminish the quality of the description of the measured intensities of the (11) and $(1\bar{1})$ beams. In the original GaAs(110) structural analysis[1] only the (01), $(0\bar{1})$, and (10) beams were analyzed. Thus the earlier analysis tended to favor a larger rotation of the top layer due to the limited data set, although the error bounds established therein encompass our present best-fit structure.

Good agreement between theory and experiment has previously been obtained using a kinematical analysis of averaged LEED intensity data by including second- and third-layer distortions of the form: first layer As up 0.26 Å, first layer Ga down 0.44 Å, second layer As down 0.06 Å, second layer Ga up 0.06 Å, third layer As up 0.03 Å, and third layer Ga down 0.03 Å, as shown by Kahn *et al.*[4] In their kinematical analysis Kahn *et al.*[4] found that the $(11)=(\bar{1}1)$ and $(0\bar{1})$ beams were the most sensitive to third-layer distortions and used the description of these beams to argue for such distortions. In order to assess the validity of their conclusions based on the kinematical structural analysis method, we have compared the intensity profiles for the structure proposed by Kahn *et al.*, and the same structure except with third-layer distortions removed for those beams which they used to obtain these distortions. The results are shown in Fig. 15. We see that the peak at 180 eV in the (11) beam occurs dynamically, even for third-layer distortions removed. This contradicts the kinematical results, as discussed by Kahn *et al.*[4] Indeed, there is little difference in intensity profiles between the two- and three-layer reconstructions [compare Fig. 15, panels (b) and (c) and panels (f) and (g)]. Thus we conclude that LEED is largely insensitive to small third-layer structural distortions, $|\Delta_{3\perp}| \leq 0.1$, even though we believe they probably occur.[15]

To summarize, the range of best single-layer distortions found was in the range of top-layer shears of 0.65–0.70 Å. Within the limits of LEED accuracy, this result is identical to the surface of Tong *et al.*,[26] [see Table I, panels (a) and (b)]. It also lies within the limits of uncertainty of the structure determined kinematically by Kahn *et al.*[3,4] We have see, however, that the dynamical electron-diffraction program is insensitive to small

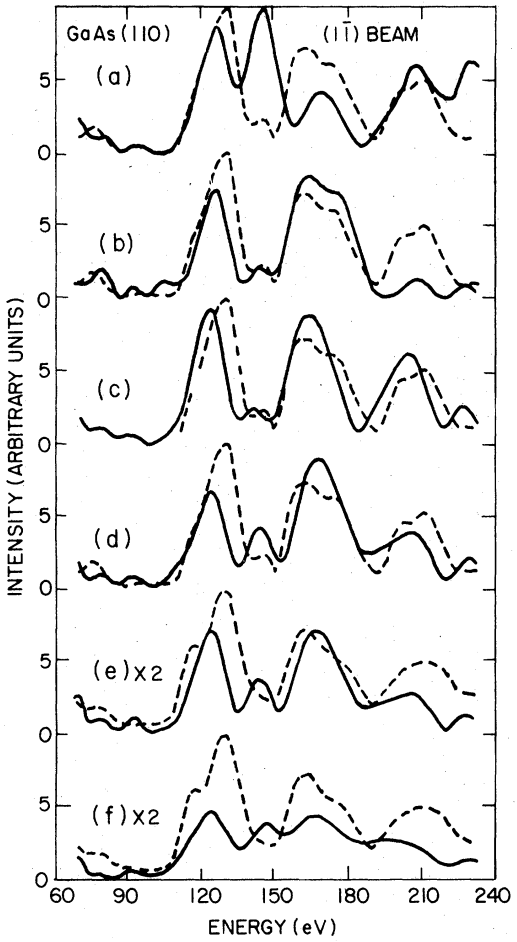

FIG. 9. Same as Fig. 5, only for the (1$\bar{1}$) beam.

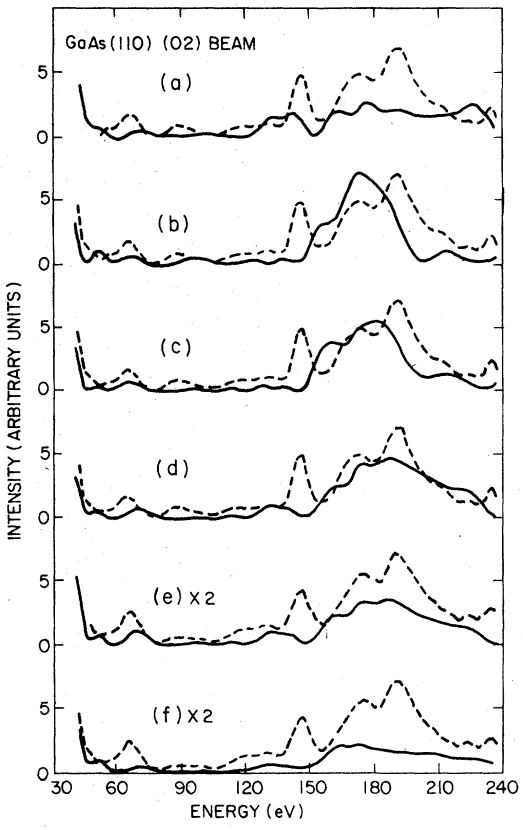

FIG. 10. Same as Fig. 5, only for the (02) beam.

third-layer distortions. In view of this contradiction between the kinematical and dynamical results, we have investigated second-layer distortions of the As and Ga sublattices with relative shears of up to $|\Delta_{21}| = 0.20$ Å, using dynamical calculations embodying the Slater-exchange model potential.

The best fit was obtained using a top layer rotated by 27.4° and contracted downward 0.05 Å, with a relative shear of the second layer of 0.12 Å obtained by moving the second-layer As downward 0.06 Å and the second layer Ga upward 0.06 Å from their positions in the bulk. This structure is identical to the second-layer reconstruction found by kinematical methods.[4] Tong *et al.*[26] concluded that the surface bilayer is contracted toward the bulk by 0.1 Å. With the second-layer reconstruction described above, a contraction by 0.1 Å was found to be too much, a significantly better value being 0.05 Å. This result is also in agreement with total energy minimization results.[15]

The intensity profiles shown in Figs. 5–14, panels (a), (b), (c), and (d), respectively, are the calculated dynamical intensities obtained from the Tong *et al.* single-layer reconstruction,[26] panel (a), from the kinematical best-fit structure of Kahn *et al.*,[4] panel (b), from the energy minimization calculation of Miller and Haneman,[16] panel (c), and from our dynamical-calculation best-fit structure, panel (d). Computer profiles for Chadi's total-energy-minimization structure[15] are not shown because they are essentially identical to those obtained using the dynamical best-fit structure. Although the single-layer reconstruction of Tong *et al.* gives a better description of a limited number of beams [compare panels (a), (b), and (d), Figs. 12 and 13], the multilayer reconstructions give a better description overall (see especially Figs. 7–10). It is noteworthy that most of these structures, shown in Table I, deviate from each other by less than the usually quoted[18,26,32] accuracy of ELEED structure analyses, i.e., $\Delta d_\perp \sim 0.1$ Å and $d_\parallel \sim 0.2$ Å. The significant structural results emanating from the dynamical multilayer analysis are the occurrence of second layer reconstructions [structure (d) is preferred over structure (a)] and the superiority of bond rotation relative to normal displacement models [structure

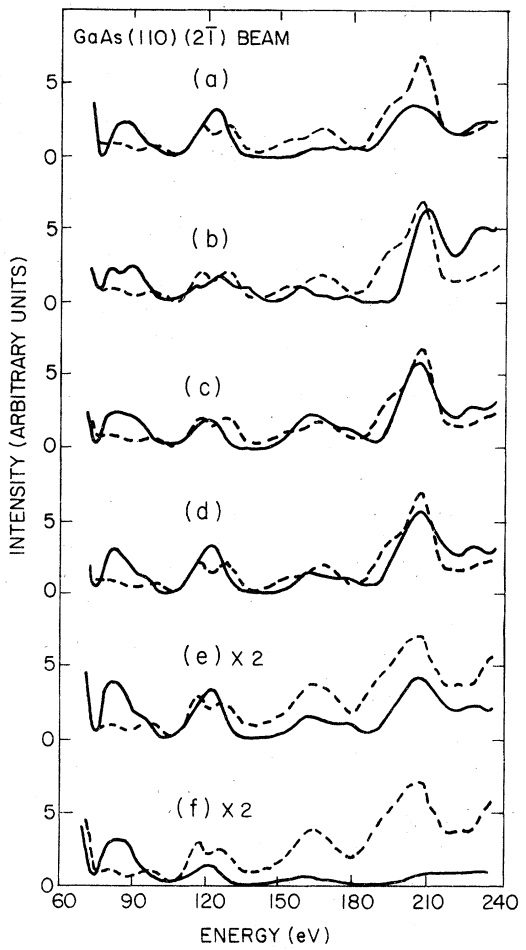

FIG. 11. Same as Fig. 5, only for the (2$\bar{1}$) beam.

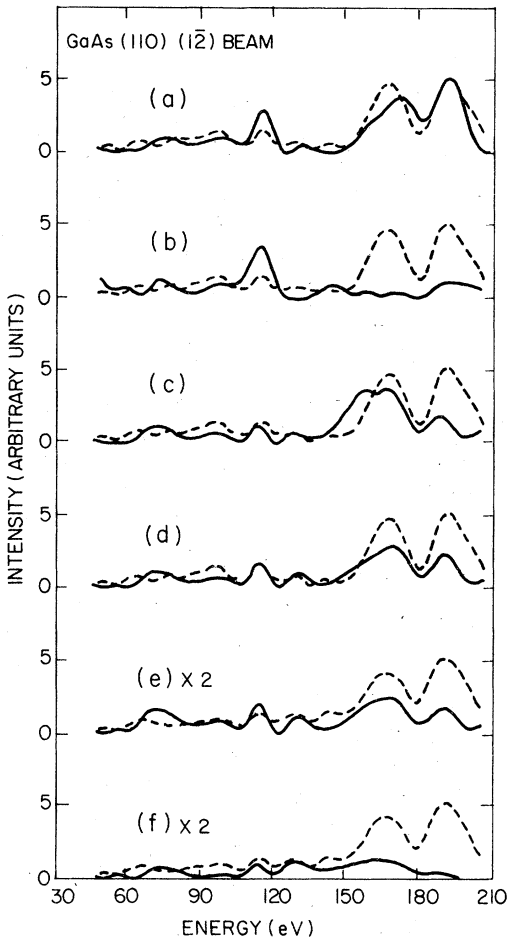

FIG. 12. Same as Fig. 5, only for the (1$\bar{2}$) beam.

(d) is preferred over structure (b)].

We conclude, therefore, that analysis of available LEED data supports the existence of second-layer structural distortions. We are unable to detect small third-layer reconstructions, however, because of the lack of sensitivity of our dynamical calculations to distortions of the size expected in the third layer.[15] Nevertheless, the first- and second-layer distortions are in excellent accord with those predicted by both total-energy[15,33] and elastic-energy[16] minimization techniques. Indeed, it is evident from Figs. 5–14 that the Miller-Haneman structure, [panel (c)] deduced from EPR data top-layer reconstructions plus elasticity-theory-determined lower-layer distortions, describes the observed intensities as well as our best-fit structure [Panels (d)–(f)]. The only previously determined structure of GaAs(110) which is clearly excluded from correspondence with our ELEED data is the 19° bond-rotation structure determined by Pandey *et al.*[34-36] on the basis of a tight-binding model analysis of angle-resolved and angle-averaged photoemission data. The corresponding value of $\Delta_{1,\perp}=0.46$ Å for the Pandey structure lies well outside the region of acceptable values of this quantity (i.e., 0.64 Å $\leq \Delta_{1,\perp} \leq$ 0.7 Å) specified by Table I and Figs. 5–14. Indeed the Pandey 19° rotated structure, as shown in Fig. 16, gives noticeably poorer correspondence with experiment than the preferred structure shown in panel (d) of Figs. 5–14. The Pandey structure lacks peaks at 150 and 210 eV in the (10) beam, a peak at 170 eV in the (1$\bar{1}$) beam, and a peak at 180 eV in the (02) beam. On the (0$\bar{1}$) and (11) beams peaks are predicted in locations where experiment shows minimum intensity. Similar results are found for other beams. Tong *et al.*[26] have performed dynamical calculations for a 20° rotated structure, and have also concluded that this structure is inconsistent with the available ELEED data. Since analyses of photoemission data lead[18] to uncertainties in $\Delta_{1,\perp}$ of as much as 0.4 Å, however, we conclude that the Pandey 19° rotated structure concurs with ours given the un-

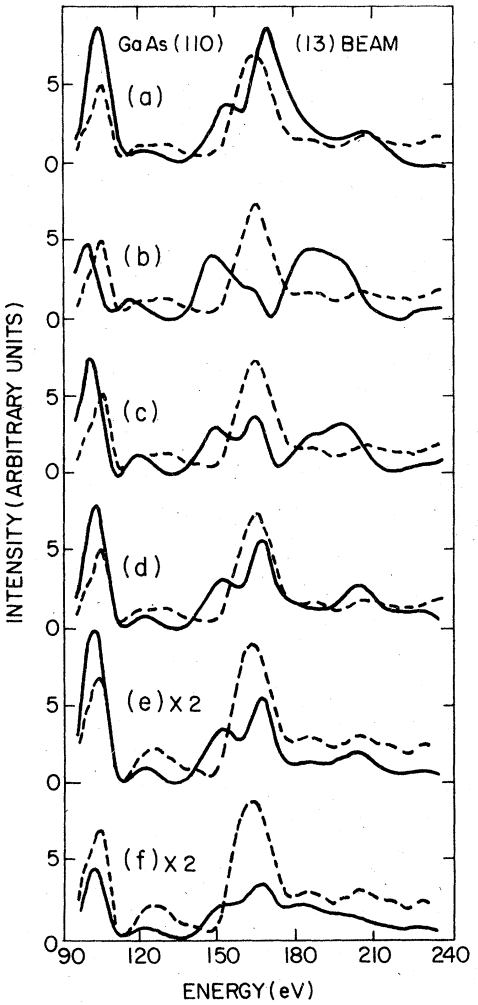

FIG. 13. Same as Fig. 5, only for the (13) beam.

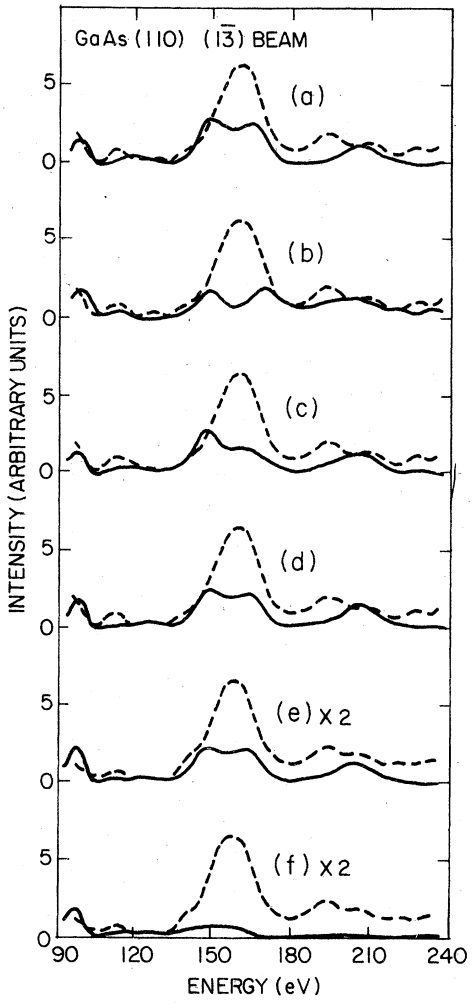

FIG. 14. Same as Fig. 5, only for the (1$\bar{3}$) beam.

certainties inherent in the photoemission analyses.

IV. SYNOPSIS

In this paper we report a new surface-structure determination for GaAs(110) via dynamical ELEED intensity analysis which represents an expansion of our earlier work in four directions. First, the sensitivity of the calculated ELEED intensities to the model exchange potential is examined. It is found that KS and Slater exchange give virtually identical agreement with experiment, in contrast to the case of metals, where KS is found to be superior. Second, the sensitivity of the intensity profiles to a new boundary condition for the treatment of spherical harmonics of complex vectors is investigated and found to have little effect. Third, the effect of surface vibrations on higher-order ELEED beams, and their implications for the magnitude of the surface Debye temperature are explored. Fourth, an extension of our matrix inversion computer program which permits an approximate treatment of multiple scattering in the bulk, but treats exactly the scattering in the surface region where reconstructions are large is reported. The resulting ELEED intensities for the most probable structures are compared with averaged data from 11 samples taken at normal incidence in Figs. 5–14.

On the basis of our model calculations we conclude that the uppermost two atomic layers are reconstructed relative to the truncated bulk-solid structure[20] given by a unit mesh $a_x = 4.00$ Å, $a_y = 5.65$ Å, and atomic positions $d_{\perp,12} = 2.00$ Å, $d_{\perp,23} = 2.00$ Å, $d_{y1}(\mathrm{Ga}) = 4.24$ Å relative to an arsenic species at the origin of the unit mesh. Specifically, we find that $d_{\perp,12}(\mathrm{As}) = 2.20 \pm 0.1$ Å, $d_{\perp,23}(\mathrm{As}) = 1.94 \pm 0.1$ Å, $d_{\perp,12}(\mathrm{Ga}) = 1.43 \pm 0.1$ Å, $d_{\perp,23}(\mathrm{Ga}) = 2.06 \pm 0.1$ Å, and $\Delta_{y1}(\mathrm{Ga}) = 4.40 \pm 0.2$ Å. These tolerances include both the multilayer re-

TABLE I. Positions of the atoms in the uppermost three atomic bilayers for those reconstructed surfaces of GaAs(110) for which calculated ELEED intensities are shown in Figs. 7–15. The symbols defining the structures are defined in the uppermost panel of Fig. 1. All distances are given in Å.

Structure	Layer	As	Ga	$\Delta_{1,\perp}$	$\Delta_{2,\perp}$	$\Delta_{3,\perp}$	$d_{12,\perp}$	$d_{23,\perp}$	$\Delta_{1,y}$	$d_{12,y}$	ω_1	Ga_1–As_1 % bond length change	Ga_1–As_2 % bond length change
Tong *et al.*	1	+0.094	+0.554										
(a)	2	0	0	0.650	0	0	1.452	1.999	4.395	3.313	27.21°	0.06	−2.50
	3	0	0										
Kahn *et al.*	1	+0.2112	+0.4888										
(b)	2	+0.06	+0.06	0.700	−0.120	0.060	1.450	2.089	4.241	2.827	26.35°	4.01	−13.71
	3	+0.03	+0.03										
Miller-Haneman	1	+0.20	+0.45										
	2	+0.05	+0.04	0.650	−0.09	0.06	1.51	2.080	4.453	3.245	28.51°	−1.22	−0.68
(c)	3	+0.02	+0.04										
Best fit	1	+0.144	+0.506										
(d)	2	+0.06	+0.06	0.650	−0.120	0.0	1.434	2.059	4.395	3.313	27.34°	0.08	0.25
	3	0.0	0.0										
Chadi	1	+0.186	+0.459										
(e)	2	+0.06	+0.07	0.645	−0.13	0.06	1.470	2.109	4.398	3.171	27.25°	−0.08	−2.87
	3	+0.02	+0.04										

[a]Reference 26. [b]Reference 4. [c]Reference 16. [d]Derived in this paper. [e]Reference 15.

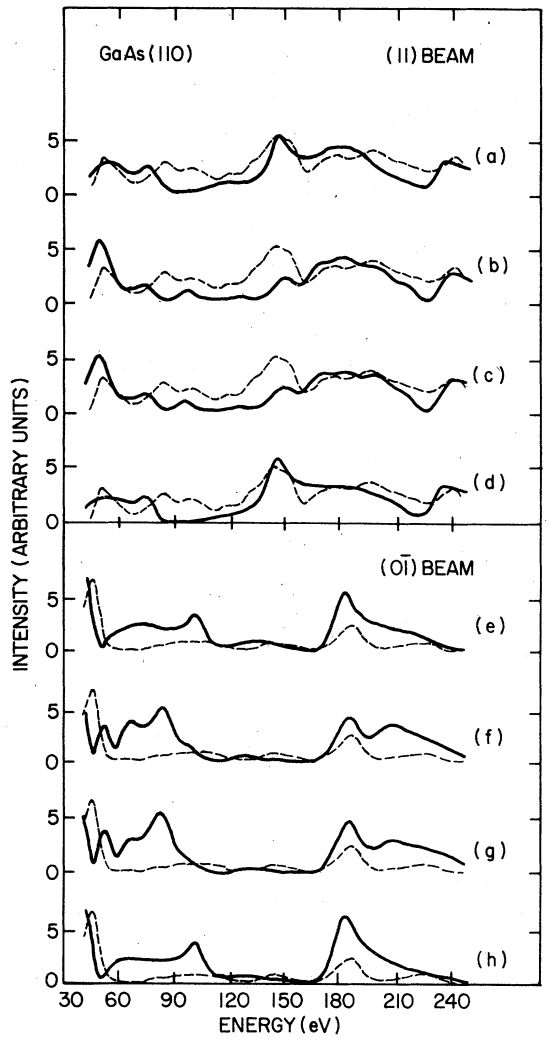

FIG. 15. Comparison of calculated [solid curves: four phase shifts, $T = 300$ K, Θ_D (surface) = 276 K] and measured (dashed curves) intensities of normally incident electrons diffracted from GaAs(110). Curve (a): the measured intensity at $T = 300$ K (dashed curve) and the kinematically calculated intensity (solid curve) using the bulk geometry of Wyckoff (Ref. 20) and the three-layer reconstruction of Kahn *et al.* (Ref. 14) for the (11) beam. Curve (b): same as curve (a), but calculated dynamically. Curve (c): same as curve (b), but no third-layer distortion. Curve (d): same as curve (c), but calculated kinematically. Curve (e): the measured intensity at $T = 300$ K (dashed curve) and kinematically calculated intensity (solid curve) using the three-layer reconstruction of Kahn *et al.* (Ref. 4) for the (0$\bar{1}$) beam. Curve (f): same as curve (e), but calculated dynamically. Curve (g): Same as curve (f), but no third distortion. Curve (h): same as curve (g), but calculated kinematically.

construction proposed for GaAs(110) by Kahn *et al.*[4] and the single layer reconstruction of Tong *et al.*[26] from an analysis of ELEED data. They also are consistent with Chadi's conclusions from

analysis of angular resolved photoemission data,[17] Chadi's energy minimized structure,[15] Miller and Haneman's hybrid EPR-energy-minimized structure,[16] and the Goddard *et al.*[33] quantum chemical calculations. While superficially they appear different from the 19° bond-rotated structure of Pandey *et al.*,[34-36] the large uncertainties inherent in the methodology used to obtain this structure render the two results compatible although not identical. The improvement in agreement between theory and experiment relative to the single-layer reconstructions of Lubinsky *et al.*[1,2] and Tong *et al.*[26] is a strong indication of the presence of second-layer reconstructions. There is, however, no dynamical ELEED evidence to support the kinematical CMTA analysis[4] indicating the presence of third layer distortions.

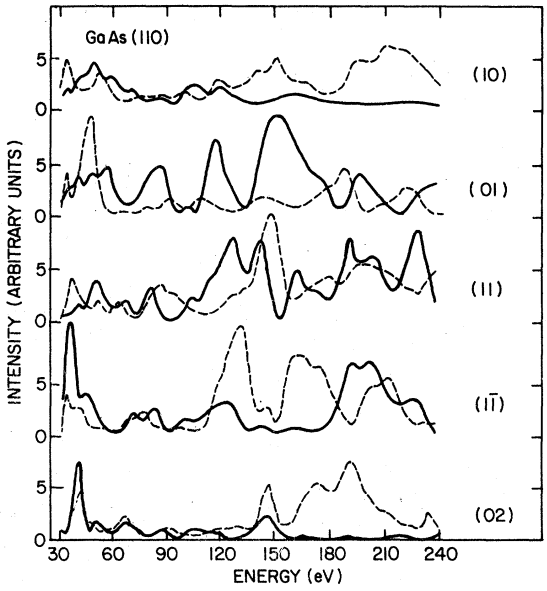

FIG. 16. Comparison of calculated (solid curves: rigid lattice, six phase shifts) and measured (dashed curves) intensities for the (10), (0$\bar{1}$), (11), (1$\bar{1}$), and (02) diffracted beams for the 19° rotated GaAs(110) reconstruction of Pandey *et al.* (Refs. 34–36).

ACKNOWLEDGMENTS

The authors are indebted to L. J. Kennedy for assistance and to M. M. Shahin and M. D. Tabak for generous support of this work. Supported by the Office of Naval Research (N00014-75-G0394), Army Research (DAAG 29-77-G-0116), National Science Foundation (NSF-ENG 75-18529), and Mobil Oil Foundation.

[1]A. R. Lubinsky, C. B. Duke, B. W. Lee, and P. Mark, Phys. Rev. Lett. 36, 1058 (1976).
[2]C. B. Duke, A. R. Lubinsky, B. W. Lee, and P. Mark, J. Vac. Sci. Technol. 13, 761 (1976).
[3]A. Kahn, E. So, P. Mark, and C. B. Duke, J. Vac. Sci. Technol. 15, 580 (1978).
[4]A. Kahn, E. So, P. Mark, C. B. Duke, and R. J. Meyer, J. Vac. Sci. Technol. 15, 1223 (1978).
[5]C. B. Duke and A. R. Lubinsky, Surf. Sci. 50, 605 (1975).
[6]G. E. Laramore and C. B. Duke, Phys. Rev. B 5, 267 (1972).
[7]A. Salwen and J. Rundgren, Surf. Sci. 53, 523 (1975).
[8]P. M. Echenique, J. Phys. C 9, 3193 (1976).
[9]S. Y. Tong, J. B. Pendry, and L. L. Kesmodel, Surf. Sci. 54, 21 (1976).
[10]W. Kohn and L. J. Sham, Phys. Rev. 140, A1133 (1965).
[11]J. C. Slater, Phys. Rev. 81, 385 (1951).
[12]C. B. Duke, N. O. Lipari, and U. Landman, Phys. Rev. B 8, 2454 (1973).
[13]C. B. Duke, in *LEED: Surface Structures of Solids*, edited by M. Laznicka (Union of Czechoslovak Mathmaticians and Physicists, Praque, 1972), Vol. 2, pp. 44–54.
[14]M. B. Webb and M. G. Lagally, in *Solid State Physics*, edited by H. Ehrenreich, F. Seitz, and D. Turnbull (Academic, New York, 1973), Vol. 28, pp. 380–394.
[15]D. J. Chadi, Phys. Rev. Lett. 41, 1062 (1978).
[16]D. J. Miller and D. Haneman, J. Vac. Sci. Technol. 15, 1267 (1978); and unpublished.
[17]D. J. Chadi, J. Vac. Sci. Technol. 15, 631 (1978); 15, 1244 (1978); Phys. Rev. B 18, 1800 (1978).
[18]C. B. Duke, Crit. Rev. Solid State Mater. Sci. 8, 69 (1978).
[19]F. Herman and Skillman, *Atomic Structure Calculations* (Prentice-Hall, Englewood Cliffs, 1963).
[20]R. W. G. Wyckoff, *Crystal Structures* (Wiley, New York, 1963), Vol. I, pp. 108–111.
[21]C. B. Duke and C. W. Tucker, Jr., Surf. Sci. 15, 231 (1969).
[22]E. Zanazzi and F. Jona, Surf. Sci. 62, 61 (1977).
[23]M. A. Van Hove, S. Y. Tong, and M. H. Elconin, Surf. Sci. 64, 85 (1977).
[24]K. O. Legg, F. Jona, D. W. Jepsen and P. M. Marcus, J. Phys. C 10, 937 (1977).
[25]C. B. Duke and G. E. Laramore, Phys. Rev. B 2, 4765 (1970); 4783 (1970).
[26]S. Y. Tong, A. R. Lubinsky, B. J. Mrstik, and M. A. Van Hove, Phys. Rev. B 17, 3303 (1978).
[27]S. Y. Tong and M. A. Van Hove, Phys. Rev. B 16, 1459 (1977).
[28]M. Born and E. Wolf, *Principles of Optics* (Pergamon, New York, 1970), pp. 615–616.
[29]C. B. Duke, R. J. Meyer, A. Paton, and P. Mark, Phys. Rev. B 18, 4225 (1978).
[30]P. Mark, S. C. Chang, W. F. Creighton, and B. W. Lee, Crit, Rev. Solid State Sci. 5, 189 (1975).
[31]C. B. Duke, R. J. Meyer, A. Paton, P. Mark, E. So, and J.-L. Yeh (unpublished).
[32]P. Mark, G. Cisneros, M. Bonn, A. Kahn, C. B. Duke, A. Paton, and A. R. Lubinsky, J. Vac. Sci. Technol. 14, 910 (1977).
[33]W. A. Goddard III, J. J. Barton, A. Redondo, and T. C. McGill, J. Vac. Sci. Technol. 15, 1274 (1978).
[34]K. C. Pandey, J. L. Freeouf, and D. E. Eastman, J. Vac. Sci. Technol. 14, 904 (1977).
[35]K. C. Pendey, J. Vac. Sci. Technol. 15, 220 (1978).
[36]J. A. Knapp, D. E. Eastman, K. C. Pandey, and F. Patella, J. Vac. Sci. Technol. 15, 1252 (1978).